Ferromagnetic resonance measurements of GaP epilayers with embedded MnP nanoclusters grown on GaP(001)

Christian Lacroix,[*] Samuel Lambert-Milot, Remo A. Masut, Patrick Desjardins, and David Ménard[†]

Regroupement québécois sur les matériaux de pointe (RQMP), Département de Génie Physique, École Polytechnique de Montréal,
C.P. 6079, succ. Centre-ville, Montréal (Québec), Canada H3C 3A7

The relation between crystallographic texture and magnetic properties of GaP epilayers with embedded MnP nanoclusters grown by metal-organic vapor phase epitaxy is investigated with angle-dependent ferromagnetic resonance (FMR) measurements. A systematic methodology entirely based on magnetic characterization identifies all the crystallographic orientations of the MnP nanoclusters relative to the GaP matrix as well as the volume fraction of MnP in each orientation. For all 18 crystallographic orientations of the MnP nanoclusters that were determined for samples grown at 650 °C, the MnP c axis is oriented along GaP $\langle 110 \rangle$. Our approach also reveals that approximately 90% of the clusters have their b axis oriented along GaP $\langle 111 \rangle$, while the remaining clusters have their b axis oriented along GaP $\langle 100 \rangle$. In addition, FMR indicates that the ratio of the anisotropy field along the intermediate magnetic axis over that of the hard magnetic axis of the embedded MnP clusters is increased by more than 20% compared to bulk MnP. Calculations suggest that a magnetoelastic and/or a surface contribution to the magnetic anisotropy of the nanoclusters is required to explain the observed difference. The methodology presented in this work is particularly suited for semiconducting epilayers with embedded nanomagnets but could be easily applied to other similar systems.

　　　　PACS number(s): 76.50.+g, 75.30.Gw, 75.50.Tt, 75.50.Pp

I. INTRODUCTION

Heterogeneous structures consisting of Mn-based submicron ferromagnets embedded in a III-V semiconducting epilayer are promising materials for the development of magnetoelectronic devices since they are compatible with present semiconductor technology and can show room-temperature ferromagnetism. Such material systems can exhibit magnetoresistance[1–4] and large magneto-optical effects.[5,6] Furthermore, Mn-based ferromagnets, such as MnAs and MnP compounds, can show high magnetocaloric effects near room temperature,[7,8] which may be of interest for refrigeration applications.

Gallium phosphide epilayers with embedded MnP nanoclusters (GaP:MnP) are especially appealing for the development of magneto-optical devices in the visible range since GaP has a wide indirect band gap (2.27 eV at 300 K) and it is nearly lattice matched to Si. In comparison, the largely studied GaAs:MnAs epilayers are confined in the infrared range (direct band gap of 1.43 eV at 300 K). MnP is orthorhombic and has a ferromagnetic-to-paramagnetic transition at 291 K.[9] It also possesses a strong biaxial magnetocrystalline anisotropy.

Gallium phosphide epilayers with embedded MnP nanoclusters were previously successfully grown using metal-organic vapor phase epitaxy (MOVPE).[10] Cross-sectional transmission electron microscopy (TEM) analyses revealed that the epilayers grown at 650 °C present no structural defects and contain quasicylindrical MnP nanoclusters that are distributed uniformly throughout the epilayer and occupy approximately 6% of the epilayer's volume.[10,11] The mean values of the main and minor axes of the nanoclusters are 30 and 24 nm with a standard deviation of 10 and 6 nm, respectively. X-ray diffraction (XRD) curves are consistent with the presence of orthorhombic MnP clusters whose c axis (3.173 Å) is oriented along the GaP $\langle 110 \rangle$ directions, b axis (5.260 Å) along GaP $\langle 111 \rangle$ or $\langle 001 \rangle$, and a axis (5.917 Å)

along GaP $\langle 11\bar{2} \rangle$ or $\langle 110 \rangle$.[11] Hall effect measurements show that the majority carriers in the GaP:MnP epilayers are holes and the carrier concentration does not exceed 10^{15} cm^{-3} at room temperature.[12]

Due to the strong biaxial magnetocrystalline anisotropy of these MnP nanomagnets, the magnetic properties of GaP:MnP epilayers strongly depend on crystallographic texture. Moreover, the semiconducting matrix surrounding the nanoclusters can modify the magnetic properties of the nanoclusters, for instance, by imposing a stress or modifying the surface of the nanoclusters. In this context, ferromagnetic resonance (FMR) measurements, which are one of the best experimental methods to measure the magnetocrystalline anisotropy of ferromagnetic materials,[13] are particularly adapted to the study of these materials.[14] Preliminary FMR measurements on GaP:MnP epilayers have revealed that the crystallographic orientations of the MnP nanoclusters relative to the GaP matrix are in agreement with XRD measurements.[11,15]

In this work, a complete characterization of the crystallographic texture of GaP:MnP epilayers is made using angle-dependent FMR measurements. Results obtained for various directions of the applied magnetic field relative to the crystal lattice of the epilayer are presented. A phenomenological model allowed us to reproduce the angular dependence of the resonance fields and therefore to determine the crystallographic orientation of the nanoclusters. The integrated intensities of the FMR peaks are used to deduce the volume fraction of nanoclusters for each crystallographic orientation. Finally, we present an analysis of the intensity of the magnetic anisotropy fields, which indicates that, in addition to the strong magnetocrystalline anisotropy, a magnetoelastic and/or surface anisotropy representing approximately 10%–20% of the total magnetic anisotropy of the MnP nanoclusters is required to explain the difference with the magnetocrystalline anisotropy of bulk MnP.

II. EXPERIMENTAL PROCEDURE

A series of 1100-nm-thick GaP:MnP epilayers were grown on semi-insulating GaP(001) substrates using a low-pressure cold-wall MOVPE reactor equipped with a fast-switching run-vent manifold using trimethylgallium (TMGa), tertiary-butylphosphine (TBP), and methyl cyclopentadienyl manganese tricarbonyl (MCTMn) as precursors, and Pd-purified hydrogen as the carrier gas.[10] The reactor pressure was set at 40 Torr with a total flow rate maintained at 4000 sccm, while the TMGa partial pressure was fixed at 2 mTorr. All samples discussed in this article were grown at a TBP/TMGa gas flow ratio maintained at 80, the MTCMn gas flow was adjusted at values of 1.00 μmole min^{-1}, and the substrate temperature was set to 650 °C. These experimental conditions provide a nominal growth rate of $\cong 1.2\ \mu$m h^{-1}.

The magnetic moment of the GaP:MnP epilayers was measured at 292 K $\pm$ 0.5 K using a vibrating sample magnetometer (VSM). The samples were mounted on a quartz rod and the hysteresis loop was measured with the magnetic field applied in the GaP [110] direction. The magnetic moment of the GaP:MnP epilayers was extracted after subtracting the magnetic moment of the substrate. The resulting value was then divided by the volume of the epilayer.

Ferromagnetic resonance curves are obtained using the FMR setup illustrated in Fig. 1. The measurements are carried out using a custom-made cylindrical cavity operating in the TE$_{011}$ mode at a frequency of 37.6 GHz (cavity loaded). The samples are glued on a quartz rod and then placed at the center of the cavity. The rod is parallel to the alternating (pumping) magnetic field H_{ac} of the cavity. The microwave generation and detection are provided by a vector network analyzer (VNA) that excites the microwave resonant cavity and measures its complex reflection coefficient R over a frequency range around

FIG. 1. Schematic representation of the FMR setup. The alternating magnetic field H_{ac} of the cavity is parallel to the rod axis and perpendicular to the static magnetic field H_0.
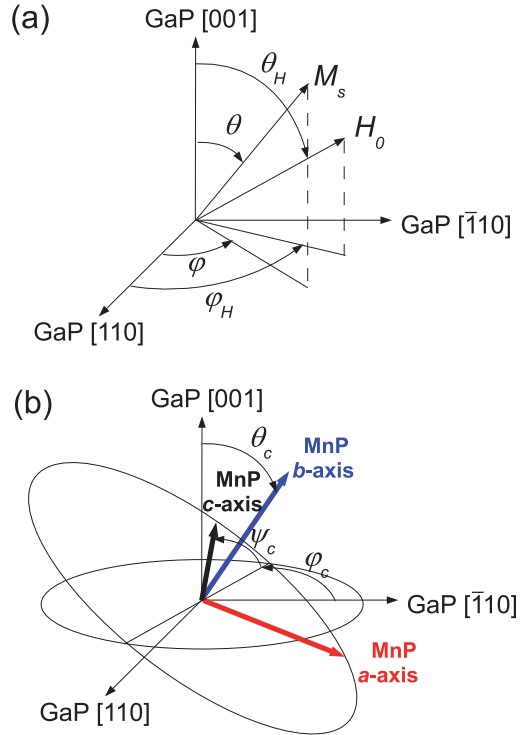
FIG. 2. (Color online) (a) The direction of the static field H_0 and the magnetization M_s relative to the GaP substrate are described by the angles (θ_H, φ_H) and (θ, φ), respectively. (b) The orientation of the MnP magnetocrystalline anisotropy relative to the GaP substrate is described by the angles ψ_c, θ_c, and φ_c.

its resonant frequency. The variation of the amplitude of the reflection coefficient ΔR at the resonant frequency of the cavity is proportional to $\eta\chi''$, where η is a filling factor corresponding to the volume of the magnetic material divided by the volume of the cavity and χ'' is the imaginary part of the sample magnetic susceptibility.[12] The proportionality constant is determined by measuring the quality factors of the resonant cavity and its coupling hole. For clarity purposes, the quantity $\eta\chi''$ will be called the experimental magnetic susceptibility (χ_{expt}). FMR curves will be presented in terms of χ_{expt} versus the applied static magnetic field H_0. The electromagnet generates a static magnetic field of up to 2 T that is perpendicular to H_{ac}. A Hall probe connected to a gaussmeter is used to monitor the static magnetic field H_0. A step motor with a belt and pulley system allows us to remotely rotate the sample in the static field from 0 to 360 °. The FMR curves of each sample are thus measured for different angles of the static field from 0 to 180 ° by steps of 0.9 °. The spherical coordinate system used to describe the direction of the magnetic field relative to the GaP substrate crystallographic orientation is presented in Fig. 2(a). All FMR measurements were carried out at 292.0 $\pm$ 0.5 K.

III. RESULTS

The magnetization of a GaP:MnP epilayer at 292 K versus a magnetic field applied in the GaP [110] direction is presented in Fig. 3. As seen in the inset, it exhibits a hysteretic behavior characteristic of the ferromagnetic phase, most probably
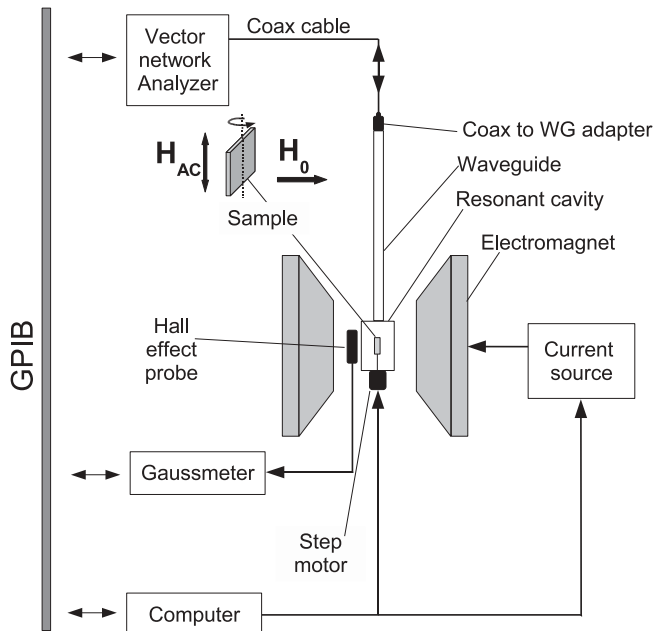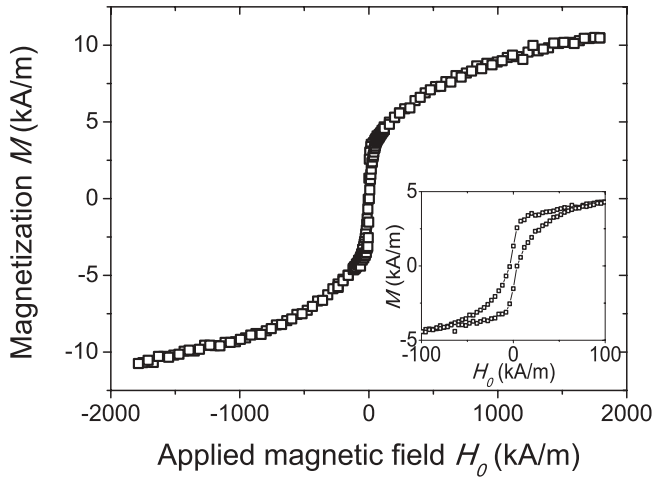
FIG. 3. Magnetization versus applied magnetic field of a GaP:MnP epilayer at 292 K with the field applied in the GaP [110] direction. The inset is a zoom of the hysteresis curve at low field.

combined with a superparamagnetic response. The GaP:MnP epilayers have a Curie temperature of 294 K, slightly above that of bulk MnP ($T_C = 291$ K).[10]

A FMR curve obtained at 37.6 GHz with the magnetic field applied in the GaP [$\bar{1}$10] direction is presented in Fig. 4 (open symbols). Three FMR peaks are observed. In order to extract the resonance field $H_{\rm res,j}$, the linewidth ΔH_j, and the area S_j of each FMR peak, the FMR curves (dimensionless) were fitted using a linear superposition of Lorentzian curves, that is,

$$\chi_{\rm expt} = \sum_{j=1}^{n} \frac{2S_j}{\pi} \frac{\Delta H_j}{4(H_0 - H_{\rm res,j})^2 + \Delta H_j^2}, \qquad (1)$$
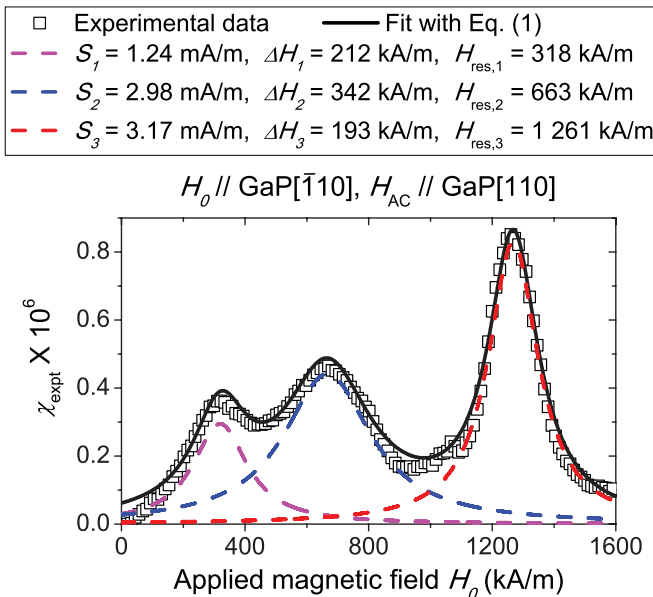
FIG. 4. (Color online) Symbols represent FMR data ($\chi_{\rm expt}$ versus applied magnetic field) obtained at 37.6 GHz and 292 K with the magnetic field applied in the GaP [$\bar{1}$10] direction. The solid line corresponds to the summation of Lorentzian curves ($n = 3$), while the dashed lines represent the individual curves.

where n is the number of peaks. All curves could be reasonably well fitted using Eq. (1) as illustrated by the solid line superposed to the FMR data presented in Fig. 4.

In Figs. 5(a)–5(d), we present two-dimensional maps of the microwave power absorbed by a GaP:MnP epilayer at 37.6 GHz and 292 K depending on the intensity and the direction of the applied magnetic field H_0 relative to the GaP crystal. The axis of rotation is parallel to four selected GaP crystallographic directions: (a) [1$\bar{1}$0], (b) [100], (c) [110], and (d) [001]. For a selected two-dimensional map, a FMR curve (obtained by varying the applied magnetic field) corresponds to a vertical line. The color scale corresponds to $\chi_{\rm expt}$, which is proportional to the power absorbed by the sample. For each map, we observe several FMR peaks whose position and shape vary strongly with the magnetic field intensity and direction. It is worth noting that while FMR curves from Figs. 5(a) and 5(c) correspond in principle to rotations around equivalent cubic lattice axes relative to the GaP substrate orientation, respectively [1$\bar{1}$0] and [110], they exhibit significantly different FMR results. Furthermore, when comparing Figs. 5(a)–5(c) with Fig. 5(d), we observe that, for the same direction of H_0 relative to the GaP substrate, the intensity also depends on the direction of $H_{\rm ac}$.

The angular dependence of the FMR peak positions, namely, the resonance fields $H_{\rm res,j}$, were obtained by fitting the curves from Figs. 5(a)–5(d) with Eq. (1). This procedure allows us to deconvolute the peaks, and obtain a better resolution of the peaks' position. The resonance fields versus the direction of the applied magnetic field are presented in Figs. 5(e)–5(h) (open circles) which better highlight peaks of lower intensity. When the axis of rotation is along GaP [1$\bar{1}$0] and [110], we noted that the values of the resonance fields are similar [see Figs. 5(e) and 5(g)]. This reveals that the difference observed in the FMR data for an axis of rotation along GaP [1$\bar{1}$0] and [110] is due to the intensities of the peaks and not their positions.

IV. ANALYSIS AND DISCUSSION OF RESULTS

It was previously proposed that each FMR peak corresponds to MnP nanoclusters whose crystal lattice is oriented along a specific GaP crystallographic direction.[15] In this section, we first develop the formalism required to model the angular dependence of the resonance fields. We then determine the crystallographic orientations and anisotropy fields of the MnP nanoclusters. Afterward, we obtain the volume fraction of MnP clusters corresponding to each crystallographic orientation from the integrated intensities of the FMR peaks. While the peaks' linewidth contains further useful information, such as the angular dispersion of MnP clusters around a crystallographic orientation, it will not be exploited in this work. Finally, we discuss the biaxial magnetic anisotropy of the MnP nanoclusters in relation to that of bulk MnP.

A. Modeling the resonance fields

Our modeling approach relies on three hypotheses. First, we treat the MnP nanoclusters as ferromagnetic single domains (macrospins) which have a saturation magnetization M_s (equal
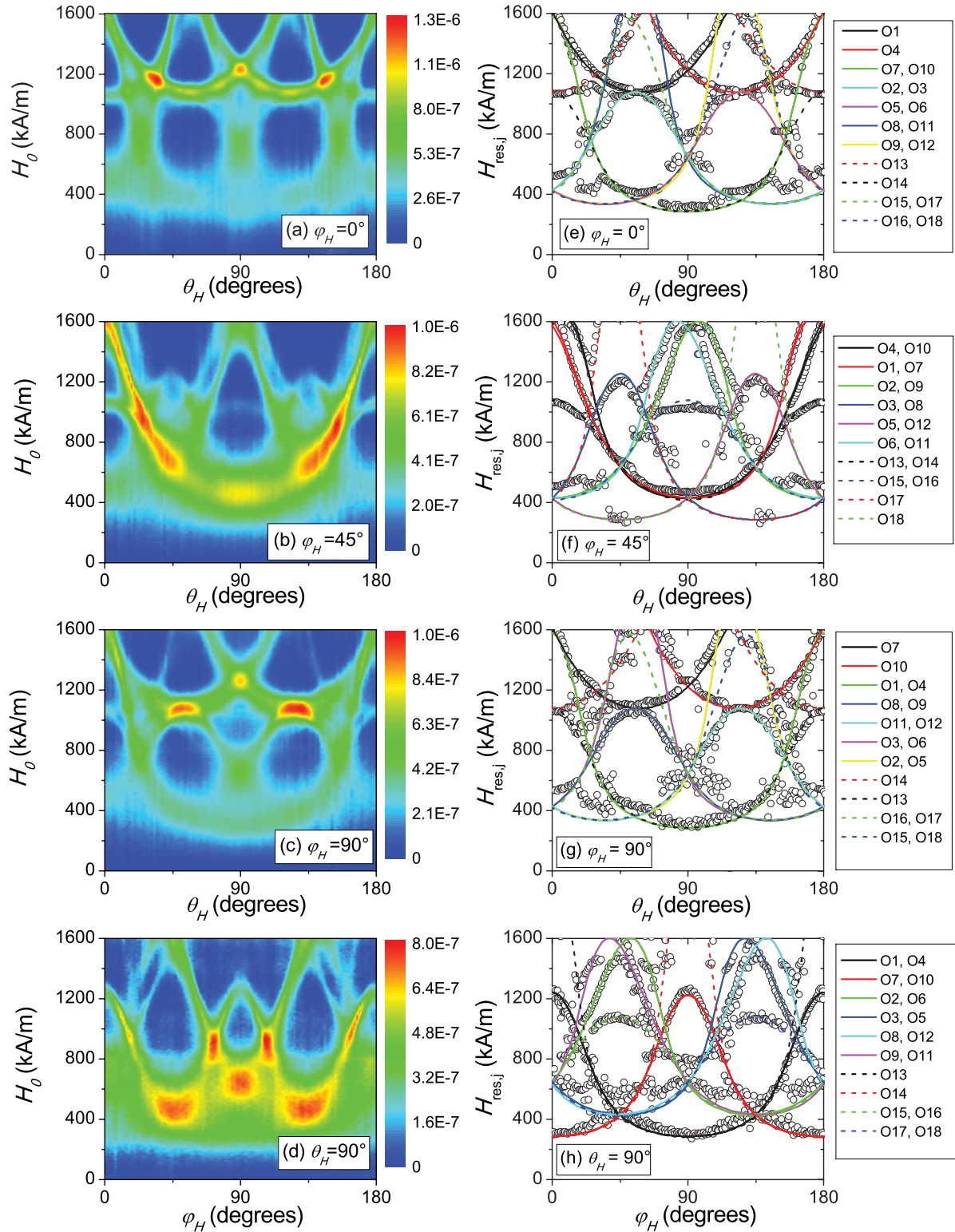
FIG. 5. (Color) Graphs on left: two-dimensional maps of the microwave power absorbed by the GaP:MnP epilayer depending on the intensity H_0 and the direction θ_H and φ_H of the applied magnetic field relative to the GaP crystal measured at 37.6 GHz and 292 K. The axis of rotation (and therefore H_{ac}) is placed parallel to different GaP crystallographic directions: (a) [1$\bar{1}$0], (b) [100], (c) [110], and (d) [001]. The color scale corresponds to χ_{expt}, which is proportional to the power absorbed by the sample. Graphs on right: angular dependence of the resonance fields $H_{res,j}$ (open circles) with the axis of rotation (and therefore H_{ac}) aligned along different GaP crystallographic directions: (e) [1$\bar{1}$0], (f) [100], (g) [110], and (h) [001]. Solid and dashed lines are fits to the data using Eqs. (2)–(6) with $H_1 = 1.25 \times 10^6$ A/m, $H_2 = 0.47 \times 10^6$ A/m, $H_3 = 0$ A/m, and $g_e = 2$.

to the spontaneous magnetization). This means that, at a constant temperature, the magnetization M_s of a cluster is considered as a vector of constant length but variable direction. The orientation of M_s is defined relative to the crystallographic orientation of the GaP(001) substrate using θ and φ, while θ_H and φ_H are used for the direction of H_0 [see Fig. 2(a)].

Second, we assume that the high-frequency susceptibility of magnetic materials can be described using the Landau-Lifshitz-Gilbert (LLG) equation.[13] For a high-frequency field H_{ac} applied perpendicularly to the static magnetic field H_0 ($H_0 \gg H_{ac}$), the magnetization precesses around the direction of the internal magnetic field H_i at a resonance angular frequency $\omega_{res} = \gamma \mu_0 H_i$, where μ_0 is the vacuum permeability and γ is the gyromagnetic ratio, which equals $g_e |e|/(2m_e)$, where g_e is the electronic g factor, e is the electron charge, and m_e is the electron mass. In the case of a ferromagnetic nanocluster, the internal magnetic field H_i corresponds to the sum of the static field H_0, the magnetocrystalline anisotropy field H_{crys}, the demagnetization field H_{dem} due to the clusters' shape, the dipolar interaction field H_{dip} between the clusters, the magnetoelastic anisotropy field H_{me} due to strains applied on the clusters, and the surface anisotropy field H_{surf}.

A convenient way to account for multiple contributions to H_i is to calculate ω_{res} using the free energy density U of all contributions. It can be shown that[13]

$$\omega_{res} = \frac{\gamma}{M_s \sin \theta_0} \left[\frac{\partial^2 U}{\partial \theta^2} \frac{\partial^2 U}{\partial \varphi^2} - \left(\frac{\partial^2 U}{\partial \theta \partial \varphi} \right)^2 \right]_{\theta_0, \varphi_0}^{1/2}, \quad (2)$$

where θ_0 and φ_0 describe the equilibrium direction of M_s.

Third, we assume that the energy density U is mainly given by the sum of the Zeeman energy density U_Z and of a triaxial (orthorhombic) magnetic anisotropy term U_a. A triaxial anisotropy has been chosen because we expect that the total anisotropy will be dominated by the strong biaxial magnetocrystalline anisotropy of orthorhombic MnP. The Zeeman energy density U_Z is expressed as follows:

$$U_Z = -\mu_0 M_s H_0 \left[\sin \theta \sin \theta_H \cos (\varphi - \varphi_H) + \cos \theta \cos \theta_H \right], \quad (3)$$

where the energy density of a triaxial anisotropy U_a is expressed as

$$U_a = K_1 A^2 + K_2 B^2 + K_3 C^2, \quad (4)$$

where

$$A = \sin \theta \cos \psi_c \cos \theta_c \cos (\varphi - \varphi_c)$$
$$+ \sin \theta \sin \psi_c \sin (\varphi - \varphi_c) - \cos \theta \cos \psi_c \sin \theta_c, \quad (5a)$$
$$B = \sin \theta \sin \theta_c \cos (\varphi - \varphi_c) + \cos \theta \cos \theta_c, \quad (5b)$$
$$C = - \sin \theta \sin \psi_c \cos \theta_c \cos (\varphi - \varphi_c)$$
$$+ \sin \theta \cos \psi_c \sin (\varphi - \varphi_c) + \cos \theta \sin \psi_c \sin \theta_c, \quad (5c)$$

and ψ_c, θ_c, and φ_c are angles used to describe the orientation of the triaxial magnetic anisotropy relative to the crystallographic

orientation of the GaP substrate [see Fig. 2(b)].[16] Including Eqs. (3) and (4) in Eq. (2), we can rearrange the terms to find[12]

$$\left(\frac{\omega_{res} M_s}{\gamma} \right)^2$$
$$= \left(\frac{\partial^2 U_Z}{\partial \theta^2} + \frac{\partial^2 U_a}{\partial \theta^2} \right) \left(\frac{\partial^2 U_Z}{\partial \theta^2} + \frac{\partial U_a}{\partial \theta} \frac{\cos \theta_0}{\sin \theta_0} \right.$$
$$\left. + \frac{\partial^2 U_a}{\partial \varphi^2} \frac{1}{\sin^2 \theta_0} \right) - \left(- \frac{\partial U_a}{\partial \varphi} \frac{\cos \theta_0}{\sin^2 \theta_0} + \frac{\partial^2 U_a}{\partial \theta \partial \varphi} \frac{1}{\sin \theta_0} \right)^2, \quad (6)$$

where

$$\frac{\partial^2 U_a}{\partial \theta^2} = 2K_1 \left(A_\theta^2 - A^2 \right) + 2K_2 \left(B_\theta^2 - B^2 \right) + 2K_3 \left(C_\theta^2 - C^2 \right), \quad (7a)$$

$$\frac{\partial U_a}{\partial \theta} = 2K_1 A A_\theta + 2K_2 B B_\theta + 2K_3 C C_\theta, \quad (7b)$$

$$\frac{\partial^2 U_a}{\partial \varphi^2} = 2K_1 \left[A_\varphi^2 - A \left(A + \cos \theta \cos \psi_c \sin \theta_c \right) \right]$$
$$+ 2K_2 \left[B_\varphi^2 - B \left(B - \cos \theta \cos \theta_c \right) \right]$$
$$+ 2K_3 \left[C_\varphi^2 - C \left(C - \cos \theta \sin \psi_c \sin \theta_c \right) \right], \quad (7c)$$

$$\frac{\partial U_a}{\partial \varphi} = 2K_1 A A_\varphi + 2K_2 B B_\varphi + 2K_3 C C_\varphi, \quad (7d)$$

$$\frac{\partial^2 U_a}{\partial \theta \partial \varphi} = 2K_1 \{ A_\theta A_\varphi + A[- \cos \theta \cos \psi_c \cos \theta_c \sin (\varphi - \varphi_c)$$
$$+ \cos \theta \sin \psi_c \cos (\varphi - \varphi_c)] \}$$
$$+ 2K_2 \{ B_\theta B_\varphi + B[- \cos \theta \sin \theta_c \sin (\varphi - \varphi_c)] \}$$
$$+ 2K_3 \{ C_\theta C_\varphi + C[\cos \theta \sin \psi_c \cos \theta_c \sin (\varphi - \varphi_c)$$
$$+ \cos \theta \cos \psi_c \cos (\varphi - \varphi_c)] \}, \quad (7e)$$

$$A_\theta = \cos \theta \cos \psi_c \cos \theta_c \cos (\varphi - \varphi_c)$$
$$+ \cos \theta \sin \psi_c \sin (\varphi - \varphi_c)$$
$$+ \sin \theta \cos \psi_c \sin \theta_c, \quad (7f)$$

$$B_\theta = \cos \theta \sin \theta_c \cos (\varphi - \varphi_c) - \sin \theta \cos \theta_c, \quad (7g)$$

$$C_\theta = - \cos \theta \sin \psi_c \cos \theta_c \cos (\varphi - \varphi_c)$$
$$+ \cos \theta \cos \psi_c \sin (\varphi - \varphi_c) - \sin \theta \sin \psi_c \sin \theta_c, \quad (7h)$$

$$A_\varphi = - \sin \theta \cos \psi_c \cos \theta_c \sin (\varphi - \varphi_c)$$
$$+ \sin \theta \sin \psi_c \cos (\varphi - \varphi_c), \quad (7i)$$

$$B_\varphi = - \sin \theta \sin \theta_c \sin (\varphi - \varphi_c), \quad (7j)$$

$$C_\varphi = \sin \theta \sin \psi_c \cos \theta_c \sin (\varphi - \varphi_c)$$
$$+ \sin \theta \cos \psi_c \cos (\varphi - \varphi_c). \quad (7k)$$

Knowing ω_{res}, the following iteration procedure is used to calculate the resonance field H_{res}. First, H_{res} is isolated in Eq. (6) and is calculated assuming that $\theta_0 = \theta_H$ and $\varphi_0 = \varphi_H$. The value of H_{res} obtained is then used to calculate θ_0 and φ_0 using the vanishing first derivatives of Eqs. (3) and (4). The values of θ_0 and φ_0 obtained are then used to recalculate H_{res} from Eq. (6). The procedure is repeated until the difference

TABLE I. MnP nanocluster crystallographic orientations described by angles φ_c, θ_c, and ψ_c and the GaP crystallographic directions which are parallel to the a, b, and c crystallographic axes of the MnP clusters. The volume fraction f of clusters for each crystallographic orientation is given. The volume fraction from the 18 orientations deduced from FMR are gathered according to their MnP c axis orientation and compared with values from Ref. 17 determined by angle-dependent magnetometry measurements.

Orientation	φ_c (deg)	θ_c (deg)	ψ_c (deg)	a axis	b axis	c axis	f (%)	f_{caxis} (%) (This work)	f_{caxis} (%) (Ref. 17)
O1	0	57	0	[11$\bar{2}$]	[111]	[$\bar{1}$10]	12.3		
O4	0	123	0	[$\bar{1}\bar{1}$2]	[11$\bar{1}$]	[$\bar{1}$10]	12.3	30	29
O13	0	0	0	[110]	[001]	[$\bar{1}$10]	5.5		
O7	90	56	0	[$\bar{1}$1$\bar{2}$]	[$\bar{1}$11]	[$\bar{1}\bar{1}$0]	13.7		
O10	90	124	0	[11$\bar{2}$]	[$\bar{1}$1$\bar{1}$]	[$\bar{1}\bar{1}$0]	13.7	29	22
O14	90	0	0	[$\bar{1}$10]	[001]	[$\bar{1}\bar{1}$0]	1.5		
O2	0	55	60	[$\bar{1}$2$\bar{1}$]	[111]	[$\bar{1}$01]	1.7		
O3	0	55	120	[$\bar{2}$11]	[111]	[0$\bar{1}$1]	1.7		
O5	0	125	60	[$\bar{2}$1$\bar{1}$]	[11$\bar{1}$]	[101]	1.7		
O6	0	125	120	[$\bar{1}$21]	[11$\bar{1}$]	[011]	1.7		
O8	90	55	60	[$\bar{2}\bar{1}$1]	[$\bar{1}$11]	[0$\bar{1}$1]	8.0		
O9	90	55	120	[$\bar{1}\bar{2}$1]	[$\bar{1}$11]	[011]	8.0	41	49
O11	90	125	60	[$\bar{1}\bar{2}\bar{1}$]	[$\bar{1}$1$\bar{1}$]	[$\bar{1}$01]	8.0		
O12	90	125	120	[$\bar{2}\bar{1}$1]	[$\bar{1}$1$\bar{1}$]	[101]	8.0		
O15	45	90	45	[$\bar{1}$0$\bar{1}$]	[100]	[$\bar{1}$01]	0.6		
O16	45	90	135	[$\bar{1}$01]	[100]	[011]	0.6		
O17	135	90	45	[0$\bar{1}\bar{1}$]	[$\bar{1}$00]	[0$\bar{1}$1]	0.6		
O18	135	90	135	[0$\bar{1}$1]	[$\bar{1}$00]	[101]	0.6		

between the values of θ_0 and φ_0 obtained from two consecutive iterations is less than 0.1%.

To fit FMR data, we replace the anisotropy constants K_1, K_2, and K_3 in Eq. (6) by the anisotropy fields $H_1 = 2K_1/(\mu_0 M_s)$, $H_2 = 2K_2/(\mu_0 M_s)$, and $H_3 = 2K_3/(\mu_0 M_s)$. This substitution eliminates the saturation magnetization M_s from the equations, which are now parametrized by H_1, H_2, H_3, and g_e.

B. Determination of the texture

Using one of the crystallographic orientations of the MnP clusters relative to the GaP substrate reported in Ref. 15, where the a axis is parallel to the GaP [11$\bar{2}$] direction, the b axis to the [111] direction, and the c axis to the [$\bar{1}$10] direction, we fitted the anisotropy fields H_1, H_2, and H_3. We found out that the following values, $H_1 = 1.25 \times 10^6$ A/m, $H_2 = 0.47 \times 10^6$ A/m, $H_3 = 0$, and $g_e = 2$, reproduce well the angular dependence of H_{res} for the FMR peak named O1 [black solid line in Fig. 5(e)]. For the rest of the paper, we will refer to a specific crystallographic orientation by using the symbols Oi, where i is a positive integer. The corresponding φ_c, θ_c, and ψ_c values are indicated in Table I. The angular dependence of H_{res} of orientation O1 was also calculated with the axis of rotation parallel to GaP [100], [110], and [001] directions [see Figs. 5(f), 5(g), and 5(h), respectively] and fitted well the corresponding experimental data points for all axes of rotation.

Considering the symmetry of the GaP crystal lattice, we established 11 other MnP clusters orientations, O2 to O12, where the MnP a axis is oriented along GaP ⟨11$\bar{2}$⟩, b axis along GaP ⟨111⟩, and c axis along GaP ⟨110⟩. Using the same values for H_1, H_2, H_3, and g_e as in the case of orientation

O1, the majority of the experimental points [solid lines in Figs. 5(e)–5(h)] were reproduced. The remaining data points can be modeled assuming MnP nanoclusters whose a axis is oriented along GaP ⟨110⟩, b axis along GaP ⟨001⟩, and c axis along GaP ⟨110⟩ (orthogonal to a) [dashed lines in Figs. 5(e)–5(h) correspond to orientations O13–O18] and using again the same values for H_1, H_2, H_3, and g_e as before. All crystallographic orientations of the MnP clusters relative to the GaP substrate discussed so far are described in Table I, where they are expressed in terms of φ_c, θ_c, and ψ_c angles. The GaP crystallographic directions parallel to the a, b, and c crystallographic axes of the MnP clusters are also presented in the third column for each orientation.

Previous work on GaAs epilayers with embedded MnAs nanoclusters (GaAs:MnAs) grown by MOVPE has shown that the MnAs c axis (or MnAs [0001] direction) was aligned along GaAs ⟨111⟩, while the MnAs [2$\bar{1}\bar{1}$0] axis was aligned along GaAs ⟨110⟩.[14] We note that even if the crystal lattice of MnP is orthorhombic, it can be seen as a slightly deformed hexagonal crystal lattice. Since the crystal lattice of MnAs is hexagonal, the correspondence between MnAs and MnP crystal lattices becomes apparent. In accordance with the terminology generally employed in the literature, the MnP b axis (or MnP [010]) corresponds to the MnAs c axis (or MnAs [0001]), while the MnP c axis (or MnP [001] direction) corresponds to MnAs [2$\bar{1}\bar{1}$0]. We can deduce that the first 12 orientations (O1–O12) listed in Table I are similar to those observed in GaAs:MnAs epilayers. In our GaP:MnP epilayers, additional crystallographic orientations (O13–O18) are present, in which the MnP c axis is also aligned along GaP ⟨110⟩, but the MnP a and b axes are now aligned along GaP ⟨110⟩ and GaP ⟨001⟩,

respectively. Note that the proportion of these orientations is rather small, as will be explained in what follows.

C. MnP volume fraction in each orientation

Since the integrated intensity S_j of a FMR peak is proportional to the magnetic moment, S_j can be used to evaluate the volume occupied by the magnetic material contributing to that resonance.[18] It is equal to $(\pi/2)\eta_j M_s$, where $\eta_j = V_j/V_c$ (j refers to a specific peak in a FMR curve), V_j is the volume occupied by the magnetic material (MnP nanoclusters), and V_c is the volume of the cavity. The ratio of the integrated intensities of two peaks can be used to deduce the ratio of the volumes occupied by the nanoclusters corresponding to each peak. Repeating this procedure using a combination of S_j values from selected peaks, the volume fraction of nanoclusters corresponding to each of the 18 crystallographic orientations can be obtained.

Some precautions are required in this procedure in order to ensure that the value corresponding to $(\pi/2)M_s/V_c$ is the same for the two peaks used when obtaining the volume ratio. Namely, the positioning of the sample in the cavity is critical since it should ideally occupy the same space in the cavity when the measurements are realized. The experimental errors due to the positioning of the sample (not a perfectly concentric quartz rod) can be minimized by comparing the integrated intensities of peaks obtained at the same angle of the static magnetic field. Next, because MnP is orthorhombic and has a strong magnetocrystalline anisotropy, the direction of the alternating field H_{ac} relative to the crystallographic orientation of MnP will affect the value of $(\pi/2)M_s/V_c$. To minimize the related error, the determination of the volume fraction requires that we compare integrated intensities from peaks with H_{ac} applied in the same crystallographic direction. With this in mind, the following procedure has been used to obtain the volume fraction occupied by the nanoclusters for each crystallographic orientation. Since there are 18 different orientations, 18 equations for the V_j variables are needed. It is straightforward to deduce the first 12 equations.[19] The method to obtain the six remaining equations to complete the system is presented below.

In Fig. 6, FMR data are fitted using Eq. (1). For each curve, FMR peaks are labeled as $P_{\alpha\beta}$, where $\alpha = a$, b, c, d, e, f, g, or h indicates the subfigure where the peak belongs, and $\beta = 1$, 2, 3, or 4 indicates the corresponding peak in the subfigure. The crystallographic orientations of the MnP clusters corresponding to each peak are also given in the legend. In Table II, the integrated intensities $S_{\alpha\beta}^{(1)}$ and $S_{\alpha\beta}^{(2)}$ of six selected pair of peaks $P_{\alpha\beta}^{(1)}$ and $P_{\alpha\beta}^{(2)}$ are presented, where the superscripts $^{(1)}$ and $^{(2)}$ distinguish the two components of one pair. Each pair of peaks provides an equation deduced from the ratio of their integrated intensities. The footnotes provide the details to deduce the remaining six equations. Using our full set of equations, the volume fractions f were calculated for each orientation and are presented in the fourth column of Table I.

According to our results from Table I, more than 90% of the clusters have their b axis oriented along GaP [111], while the remaining clusters have their b axis oriented along GaP [100].

Also, we note that even if orientations O2, O3, O5, and O6 are, considering the cubic symmetry of GaP lattice, supposedly equivalent to orientations O8, O9, O11, and O12, there is a large difference in the associated volume fraction. The well-known different chemical bonding configuration of the zinc-blende GaP growth planes is most probably the reason for this difference.[11] Similar observations are made with orientations O1 and O4 with O7 and O10 and orientations O13 with O14.

Recent angle-dependent magnetometry measurements on the samples are consistent with MnP nanoclusters having their c axis oriented along GaP $\langle 110 \rangle$.[17] Fitting of the angular dependence of the remanent magnetization was used to determine the MnP volume fraction of each MnP c axis orientation. In Table I, we have gathered the volume fraction of the 18 orientations Oi deduced from FMR in three groups according to the MnP c axis orientations found in our samples. The results are compared with those found with angle-dependent magnetometry.[17] We see that both methods yield similar results. The difference observed in values can be attributed to the experimental and fitting errors of both methods. We estimate that the absolute error on the volume fraction percentages obtained from FMR measurements ($f_{c\,\mathrm{axis}}$) is roughly 5%, based on the relative errors of S_j values obtained from the fit of FMR curves with Eq. (1). Considering that the error from magnetometry measurements is expected to be of the same order, results from both approaches are in fair agreement.

D. Modified biaxial magnetic anisotropy

It is of interest to compare the anisotropy field values of MnP nanoclusters embedded in a GaP epilayer, extracted from the FMR curves, with those of bulk MnP found in the literature. However, the anisotropy and magnetization of bulk MnP varies significantly as a function of temperature around the Curie point and, since the Curie point of the MnP nanoclusters is different from that of the bulk, it is meaningless to compare the two. Alternatively, one may compare the H_2/H_1 ratio value of bulk MnP from Ref. 9 with that of MnP nanoclusters embedded in a GaP epilayer. For the temperature range considered, the ratio for bulk MnP is approximately constant as a function of temperature with a value of 0.30, while it is 0.37 ± 0.01 for the MnP nanoclusters. This may indicate the presence of an additional contribution to the magnetic anisotropy for MnP nanoclusters embedded in a GaP epilayer, besides that of the dominating biaxial magnetocrystalline anisotropy of bulk MnP. In order to be coherent with the fact that a biaxial anisotropy is required to fit the angle-dependent resonance field, this additional magnetic anisotropy field H_{add} must be parallel to one of the MnP magnetocrystalline anisotropy axes a, b, or c. Assuming that H_{add} is present along only one of the MnP crystallographic axes, we deduce that H_{add} should equal -300, 88, or -156 kA/m, according to whether it would be parallel to the a, b, or c axes, respectively.

We can think of four different possible origins for H_{add}: shape (H_{dem}), dipolar interaction between nanoclusters (H_{dip}), magnetoelastic contribution (H_{me}), and surface anisotropy (H_{surf}). We will investigate all four possibilities.

Let us first consider shape effects. TEM images show that the shape of MnP nanoclusters is quasicylindrical, with their
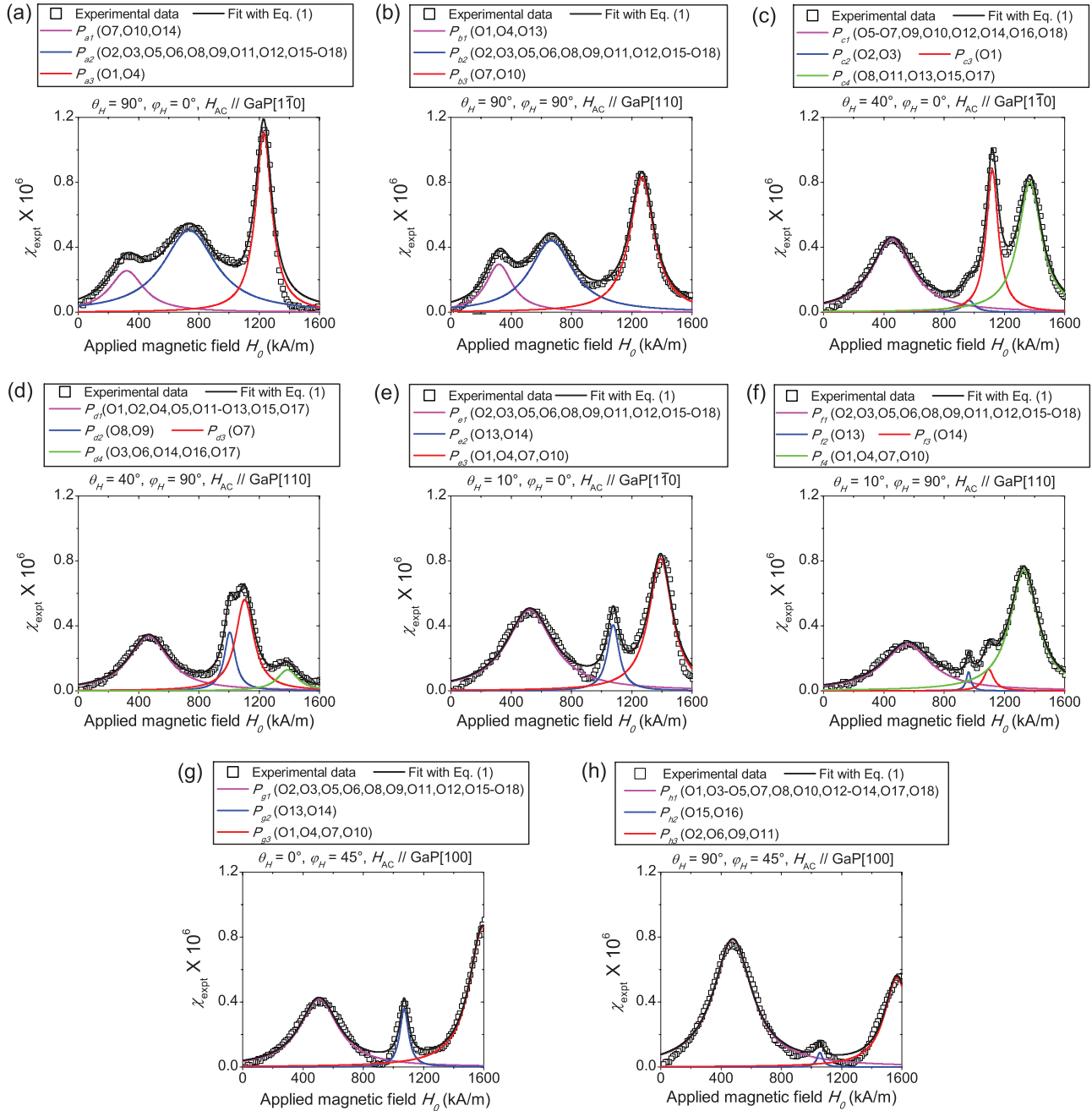
FIG. 6. (Color online) Fitting of FMR curves used to determine the volume fraction occupied by the clusters for each of the 18 crystallographic orientations.

main axis oriented along GaP $\langle 110 \rangle$.[10] From our previous results (see Sec. IV B), this means that the cylinder axis is parallel to the MnP crystallographic c axis. Considering that the average ratio of the length of the main axis on the minor axis is about 1.3, we can deduce, by approximating the cylindrical shape with a prolate ellipsoid shape, that the demagnetizing factor in the direction of the main axis $N_\parallel = 0.27$ and that the demagnetizing factor in the direction perpendicular to the main axis $N_\perp = 0.365$.[20] From Fig. 3, we evaluate the saturation magnetization M_s of the GaP:MnP epilayer at $T = 292$ K to be ≈ 11 kA/m. Considering that the volume occupied by the MnP

clusters is roughly 6%, we obtain a saturation magnetization for the MnP nanoclusters of 185 kA/m at $T = 292$ K. We can then calculate the demagnetizing field $H_{\text{dem}} = (N_\parallel - N_\perp)M_s$, which gives an intensity, in absolute value, of about 18 kA/m. This value is too small to explain the difference between the two H_2/H_1 ratios.

Second, the dipolar interaction between the MnP nanoclusters will induce a magnetic anisotropy due to the shape of the GaP:MnP sample (thin film). Using a similar procedure as described in Ref. 21, it is straightforward to find an expression allowing us to calculate H_{dip} in the case of

TABLE II. Integrated intensities of selected peaks used for the determination of the volume fraction occupied by the clusters of each crystallographic orientation. The relative error on $S_{\alpha\beta}^{(1)}$ and $S_{\alpha\beta}^{(2)}$ is approximately $\pm 7.5\%$ based on the confidence of the fit of FMR curves with Eq. (1).

$P_{\alpha\beta}^{(1)}$	$S_{\alpha\beta}^{(1)}$ (mA/m)	$P_{\alpha\beta}^{(2)}$	$S_{\alpha\beta}^{(2)}$ (mA/m)	$S_{\alpha\beta}^{(1)}/S_{\alpha\beta}^{(2)}$
P_{a3} (O1, O4)	$S_{a3} = 2.82$	P_{b3} (O7, O10)	$S_{b3} = 3.17$	0.89[a]
P_{c2} (O2, O3)	$S_{c2} = 0.13$	P_{d2} (O8, O9)	$S_{d2} = 0.62$	0.21[b]
P_{e2} (O13, O14)	$S_{e2} = 0.75$	P_{f3} (O14)	$S_{f3} = 0.21$	3.57[c]
P_{c3} (O1)	$S_{c3} = 1.65$	P_{e2} (O13, O14)	$S_{e2} = 0.75$	2.20[d]
P_{g2} (O13, O14)	$S_{g2} = 0.49$	P_{h2} (O15, O16)	$S_{h2} = 0.08$	6.12[e]
P_{g3} (O1, O4, O7, O10)	$S_{g3} = 3.08$[f]	P_{h3} (O2, O6, O9, O11)	$S_{h3} = 2.16$	1.43[g]

[a]Gives $V_{O1} = 0.89 V_{O7}$, since $V_{O1} = V_{O4}$ and $V_{O7} = V_{O10}$.
[b]Gives $V_{O2} = 0.21 V_{O8}$, since $V_{O2} = V_{O3}$ and $V_{O8} = V_{O9}$.
[c]Gives $(V_{O13} + c V_{O14}) = 3.57 V_{O14}$. The factor c is added to take into account the fact that H_{ac} is not in the same direction for V_{O13} and V_{O14}. With $c A_{f2} = c A_{O13} = 0.09$ mA/m and $A_{f3} = A_{O14} = 0.21$ mA/m, we deduce that $c = 0.025$ and therefore, we obtain $V_{O13} = 3.55 V_{O14}$.
[d]Gives $V_{O1} = 2.20 (V_{O13} + c V_{O14})$. With $c = 0.025$ and $V_{O13} = 3.55 V_{O14}$, we obtain $V_{O1} = 2.22 V_{O13}$.
[e]Gives $(V_{O13} + V_{O14}) = 6.12 (V_{O15} + V_{O16})$. With $V_{O13} = 3.55 V_{O14}$ and $V_{O15} = V_{O16}$, we obtain $V_{O13} = 9.55 V_{O15}$.
[f]Average of integrated intensities obtained at $\theta_H = 0°$ and $\theta_H = 180°$ [(3.74 + 2.41)/2 = 3.08].
[g]Gives $(V_{O1} + V_{O4} + V_{O7} + V_{O10}) = 1.43 (V_{O2} + V_{O6} + V_{O9} + V_{O10})$. With $V_{O1} = V_{O4}$, $V_{O7} = V_{O10}$, $V_{O1} = 0.89 V_{O7}$, $V_{O2} = V_{O6}$, $V_{O9} = V_{O11}$, and $V_{O2} = 0.21 V_{O9}$, we obtain $V_{O1} = 7.35 V_{O2}$.

GaP:MnP epilayers.[12] Using $M_s = 185$ kA/m, we find $H_{dip} = 9.1$ kA/m, which is also too small to explain the difference between the H_2/H_1 ratios.

Consider now the magnetoelastic anisotropy. According to XRD measurements, the deformation $\Delta l/l$ of the clusters' crystal lattice relative to bulk MnP along the a, b, and c axes is approximately -1.4%, 1.3%, and 0.8%, respectively, at $T = 292$ K.[22] The linear compressibility of bulk MnP at 292 K is 1.6×10^{-12} m^3/J along the a and b axes and 5.2×10^{-12} m^3/J along the c axis.[23] Therefore, the corresponding imposed stress σ required to deform the clusters is -8.8×10^9 J/m^3 along the a axis, 8.1×10^9 J/m^3 along the b axis, and -1.5×10^9 J/m^3 along the c axis. Taking $|\lambda_s| \approx 1 \times 10^{-5}$, which is a typical value for ferromagnetic metals, and the anisotropy field due to a magnetoelastic contribution to be equal to $3\lambda_s \sigma/(\mu_0 M_s)$,[24] we roughly estimate the intensity of H_{me} to be (in absolute value) 1.1×10^6 A/m along the a axis, 1.0×10^6 A/m along the b axis, and 0.19×10^6 A/m along the c axis, which would be sufficiently large to explain the modified magnetocrystalline anisotropy.

In the case of surface anisotropy, the corresponding energy is equal to $C K_s S$, where C is a dimensionless constant whose value is between 0 and 1 depending on the particle shape, K_s is the surface anisotropy constant, and S is the surface area.[25] The surface anisotropy field H_{surf} thus equals $2C K_s S/(\mu_0 M_s V)$, where V is the volume of the particle. Deducing the average values of C and V for the MnP nanoclusters from TEM images, and assuming a typical value $|K_s| = 0.5$ mJ/m^2, we obtain (in absolute value) $H_{surf} \approx 700$ kA/m, indicating that a contribution from the surface to the magnetic anisotropy can not be ruled out.

From our estimates, we deduce that cluster shape or dipolar interactions cannot explain the observed modifications of the magnetic anisotropy, and both the magnetoelastic and surface contributions are estimated to exhibit the right order of magnitude to be the cause of the modified magnetic anisotropy observed from MnP nanoclusters embedded in a GaP epilayer.

V. SUMMARY

In this work, we have shown that it is possible to determine the crystallographic texture of semiconducting epilayers with embedded ferromagnetic nanoclusters using ferromagnetic resonance measurements. The resonance fields were used to determine the crystallographic orientation of the nanoclusters relative to the GaP substrate. Specifically, the angle dependence of the resonance fields was fitted using a phenomenological model which assumes a biaxial magnetic anisotropy, similar to the magnetocrystalline anisotropy of bulk MnP. The modeling of the data enabled us to find all crystallographic orientations among which the nanoclusters are distributed. Also, analysis of the integrated intensities of the FMR peaks allowed us to deduce the volume fraction occupied by the clusters for each crystallographic orientation. The results obtained from the approach presented in this work are in agreement with the results obtained from structural characterization provided by XRD.[11]

In addition to the determination of the crystallographic texture, FMR enabled the determination of other magnetic properties such as the magnetic anisotropy fields. It was determined that for the case of the biaxial magnetic anisotropy, the ratio H_2/H_1 of MnP nanoclusters embedded in a GaP epilayer differs from that of bulk MnP. Our calculations show that only a magnetoelastic and/or surface anisotropy could explain this discrepancy. Finally, our work highlights the importance of crystallographic texture and the structural properties of these materials on their magnetic properties.

*christian.lacroix@polymtl.ca

†david.menard@polymtl.ca

[1] P. J. Wellmann, J. M. Garcia, J.-L. Feng, and P. M. Petroff, Appl. Phys. Lett. **73**, 3291 (1998).

[2] W. Heimbrodt, P. Klar, S. Ye, M. Lampalzer, C. Michel, S. Baranovskii, P. Thomas, and W. Stolz, J. Supercond. **18**, 315 (2005).

[3] P. N. Hai, S. Ohya, M. Tanaka, S. Barnes, and S. Maekawa, Nature (London) **458**, 489 (2009).

[4] M. Elm, C. Michel, J. Stehr, D. Hofmann, P. Klar, S. Ito, S. Hara, and H.-A. von Nidda, J. Appl. Phys. **107**, 013701 (2010).

[5] H. Akinaga, S. Miyanishi, K. Tanaka, W. van Roy, and K. Onodera, Appl. Phys. Lett. **76**, 97 (2000).

[6] G. Monette, C. Lacroix, S. Lambert-Milot, V. Boucher, D. Ménard, and S. Francoeur, J. Appl. Phys. **107**, 09A949 (2010).

[7] H. Wada and Y. Tanabe, Appl. Phys. Lett. **79**, 3302 (2001).

[8] R. Booth and S. Majetich, J. Appl. Phys. **105**, 07A926 (2009).

[9] E. Huber and D. Ridgley, Phys. Rev. **135**, A1033 (1964).

[10] S. Lambert-Milot, C. Lacroix, D. Ménard, R. A. Masut, P. Desjardins, M. Garcia-Hernandez, and A. de Andres, J. Appl. Phys. **104**, 083501 (2008).

[11] S. Lambert-Milot, S. Gaudet, C. Lacroix, D. Ménard, R. A. Masut, P. Desjardins, and C. Lavoie, J. Vac. Sci. Technol. A **30**, 061510 (2012).

[12] C. Lacroix, Ph.D. thesis, École Polytechnique de Montréal, 2010.

[13] A. G. Gurevich and G. A. Melkov, *Magnetization Oscillations and Waves* (CRC Press, Boca Raton, 1996).

[14] H.-A. Krug von Nidda, T. Kurz, A. Loidl, T. Hartmann, P. Klar, W. Heimbrodt, M. Lampalzer, K. Volz, and W. Stolz, J. Phys.: Condens. Matter **18**, 6071 (2006).

[15] C. Lacroix, S. Lambert-Milot, P. Desjardins, R. A. Masut, and D. Ménard, J. Appl. Phys. **103**, 07D531 (2008).

[16] In this work, a positive value of the anisotropy constant K_i ($i = 1,2,3$) corresponds to a hard magnetic axis. We note that it is straightforward to demonstrate that only two anisotropy constants are required to represent a biaxial anisotropy. In Eq. (4), we use three anisotropy constants for completeness, but later take $K_3 = 0$ in the application.

[17] C. Lacroix, S. Lambert-Milot, P. Desjardins, R. A. Masut, and D. Ménard, J. Appl. Phys. **105**, 07C119 (2009).

[18] M. Farle, Rep. Prog. Phys. **61**, 755 (1998).

[19] Because of symmetric considerations, the following equalities are inferred: $V_{O1} = V_{O4}$, $V_{O2} = V_{O3} = V_{O5} = V_{O6}$, $V_{O7} = V_{O10}$, $V_{O8} = V_{O9} = V_{O11} = V_{O12}$, and $V_{O15} = V_{O16} = V_{O17} = V_{O18}$, where V_{Oi} is the volume occupied by the clusters from orientation Oi. This is clearly seen by the twofold symmetry of the two-dimensional maps presented in Fig. 5.

[20] J. Osborn, Phys. Rev. **67**, 351 (1945).

[21] L.-P. Carignan, C. Lacroix, A. Ouimet, M. Ciureanu, A. Yelon, and D. Ménard, J. Appl. Phys. **102**, 023905 (2007).

[22] S. Lambert-Milot, Ph.D. thesis, École Polytechnique de Montréal, 2012.

[23] N. Iwata, J. Sci. Hiroshima Univ., Ser. A **33**, 1 (1969).

[24] R. C. O'Handley, *Modern Magnetic Materials: Principles and Applications* (Wiley, New York, 2000).

[25] J. M. D. Coey, *Magnetism and Magnetic Materials* (Cambridge University Press, Cambridge, UK, 2010).